ACADEMIC PRESS

Available online at www.sciencedirect.com
SCIENCE DIRECT®

Journal of Catalysis 219 (2003) 117–125

JOURNAL OF CATALYSIS

www.elsevier.com/locate/jcat

Effect of local framework heterogeneity on NO adsorption in cobalt–ferrierite

Scott A. McMillan, Linda J. Broadbelt,* and Randall Q. Snurr *

Northwestern University, Institute for Environmental Catalysis and Department of Chemical Engineering, 2145 Sheridan Road, Evanston, IL 60208-3120, USA

Received 24 October 2002; revised 11 April 2003; accepted 22 April 2003

Abstract

Quantum chemical calculations have been performed to evaluate the adsorption of NO on cobalt in several extraframework environments within ferrierite zeolites. All possible arrangements of the two nearby framework aluminum atoms have been considered for the B and G ferrierite cobalt sites. The cobalt–nitrosyl orientation, i.e., bent versus linear, depends on the local zeolite environment. The enthalpies and free energies of adsorption are also functions of the local zeolite environment. NO adsorption is favored by about 50 kJ/mol on cobalt in the B site compared to the G site. This large difference is attributable to two factors: differences in NO-induced strain on the cobalt–zeolite environments as well as an intrinsic difference based on the coordinative unsaturation of cobalt. A simulation of the temperature-programmed desorption profile reveals three distinct cobalt environments for adsorbed NO, showing the dependence of a macroscopic property that is related to catalytic activity on the local zeolite environment near a metal cation. This observation suggests that the increase in the turnover of NO to N_2 per cobalt atom with increasing cobalt loading reported in the literature may be related to the same factors. A detailed analysis of the cobalt–nitrosyl bond was also performed.

Keywords: Cobalt; Zeolite; Nitrosyl; Density functional theory; SCR catalysis

1. Introduction

In order for present automobile catalytic converters to operate properly, engines must operate near the air/fuel stoichiometric ratio to minimize the amount of oxygen in the exhaust. Lean-burn engines are more fuel efficient but operate at higher air/fuel ratios than standard engines. However, the popular three-way catalyst is unable to remove nitrogen oxides (NO_x) from the oxygen-rich lean-burn exhaust. Preferentially reducing NO_x requires new, selective catalysts. Zeolite-based materials exchanged with transition metals selectively catalyze the reduction of NO_x with hydrocarbon reducing agents in the presence of excess oxygen [1] and are being studied extensively for automotive applications.

Cobalt-exchanged zeolites are particularly notable for their high selective catalytic reduction (SCR) activity [2,3]. The initial research into cobalt-exchanged ferrierite also established that the SCR activity is a function of the cobalt loading. The turnover frequency of NO to N_2 per cobalt is not constant, but *increases with the amount of cobalt exchanged* [4]. Subsequent research has established that ion exchange from aqueous solution results in isolated divalent cobalt cations [5–8].

Since only one form of exchanged cobalt is present in these catalysts, the siting of cobalt in ferrierite must control the increase in the turnover frequency. The distribution of cobalt in the zeolite extraframework sites is a function of the cobalt loading [9]. Different local zeolite environments around cobalt certainly affect the SCR activity of individual cobalt cations, although it is not known to what degree. Alternatively, the SCR mechanism may be enhanced by a synergistic cooperation between nearby cobalt ions [10,11]. The probability of nearby cobalt cations increases with the cobalt loading. Quantifying either of these interactions requires detailed knowledge about the extraframework siting of cobalt.

Wichterlová and co-workers have observed three spectroscopic signatures, designated α, β, and γ, for cobalt in

* Corresponding authors.
E-mail addresses: broadbelt@northwestern.edu (L.J. Broadbelt), snurr@northwestern.edu (R.Q. Snurr).

0021-9517/$ – see front matter
doi:10.1016/S0021-9517(03)00196-9

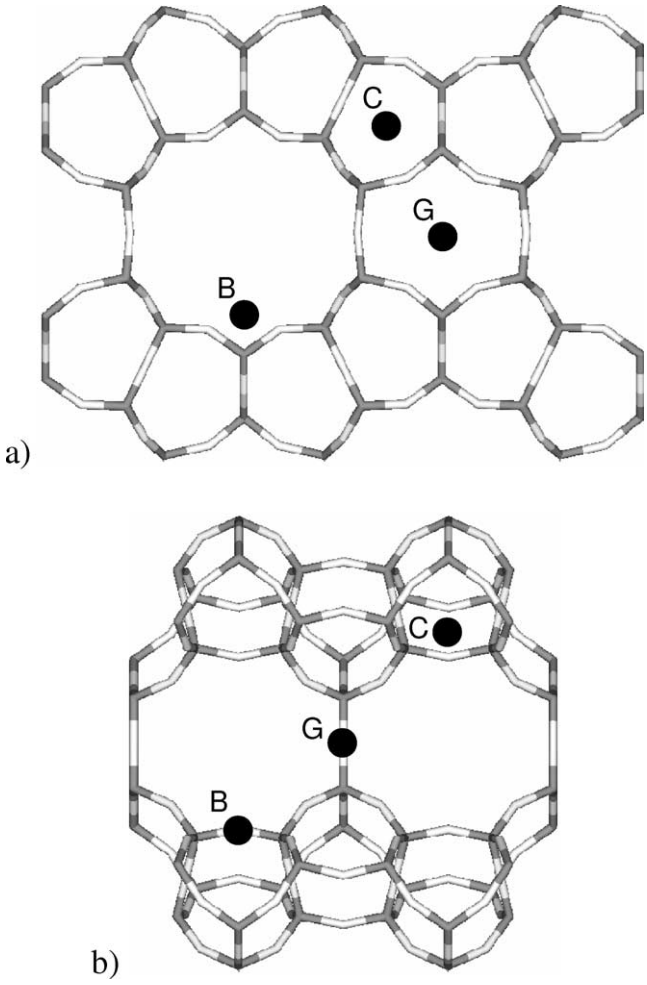

Fig. 1. Location of extraframework sites B, C, and G in ferrierite (a) looking down the 10-ring channels and (b) looking down the 8-ring channels.

ferrierite [9]. The intensity of each of these signatures varies with the Co/Al ratio. The majority of exchanged cobalt has the β signature at all loadings, a significant minority has the α signature, while the γ signature usually accounts for a small fraction of cobalt. Further, they suggested specific extraframework cobalt sites for each signature. The signatures have been proposed to correspond one-to-one with ferrierite extraframework sites B, G, and C, respectively, using the notation of Mortier [12] (Fig. 1). This assignment was made based on indirect spectroscopic evidence and may need to be refined in light of recent density functional theory (DFT) calculations [13]. The relative arrangement of framework aluminum atoms in the extraframework site is fundamental to the siting of cobalt, as well as other divalent metals [14,15]. For example, only one arrangement of aluminum atoms in the G site, denoted G-1,3 below, reproduced all of the experimental β signature data in the DFT work [13]. Several aluminum arrangements in both the B and the G sites gave rise to the α signature.

In this work, calculations related to the catalytic activity have been performed for the same metal in different zeolite extraframework environments. The adsorption of NO is presumably one of the first steps in the overall NO_x SCR mechanism. We show that the formation of mononitrosyl adsorption complexes depends on the cobalt coordination environment. The eight cobalt environments considered here fall into three classes based on their atomic-scale and macroscopic properties. These results demonstrate one way that the catalytic activity of cobalt may depend on the local zeolite environment.

2. Theoretical methods

The B site is located at the wall of the 10-ring channel near the intersection of the 8- and 10-ring channels, and the G site is a 6-membered ring separating two 8-ring channels (Fig. 1). The C site is a boat-shaped site; cobalt exhibiting the γ signature is present only in very low quantities [16] and hence was not considered. Isolated divalent cations require two nearby framework aluminum atom substitutions for charge compensation. All four unique two-aluminum substitutions for the B and G ferrierite sites have been previously investigated for cobalt in the absence of adsorbed molecules [13]. Briefly, for the B and G sites, four such symmetrically distinct arrangements are possible, denoted (1,3), (1,4), (2,5), and (2,6). The calculated properties, including the spectroscopic signature, depend strongly on the relative aluminum arrangement.

In this work, the same eight cluster models extracted from the ferrierite framework were used to investigate cobalt–mononitrosyl formation as shown in Figs. 2–5. The atoms at the edge of each cluster were terminated by hydrogen atoms directed along the bond vector of what would have been the next zeolite framework atom. The Si–H and O–H distances were fixed at 1.49 and 0.98 Å, respectively. The Cartesian positions of the terminating OH and SiH_3 groups were constrained while the rest of the cluster and NO were allowed to relax fully. In all of the clusters, NO, the entire six-member ring, and all the oxygen atoms coordinated to the aluminum atoms are allowed to relax. In the B sites, the atoms that are part of the fused five-member rings are also allowed to relax (i.e., the Al–O–Si–O–Al bridge in the B-1,4 environment). The cluster size has been shown to retain enough flexibility to describe the interaction of cobalt with ferrierite [13]; trial calculations on larger clusters and clusters with different terminating groups did not significantly change any of the calculated properties. An additional environment, Co^{2+} surrounded by four water molecules (Fig. 6), was also investigated. The properties of the cobalt environments were determined through the application of density functional theory using the BP86 gradient-corrected functional [17,18]. The LANL2DZ effective core potential basis set was used for all of the calculations. The LANL2DZ basis replaces the 1s through 2p electrons of the heavy atoms with a potential field for a considerable computational savings. A double-ζ quality Dunning basis

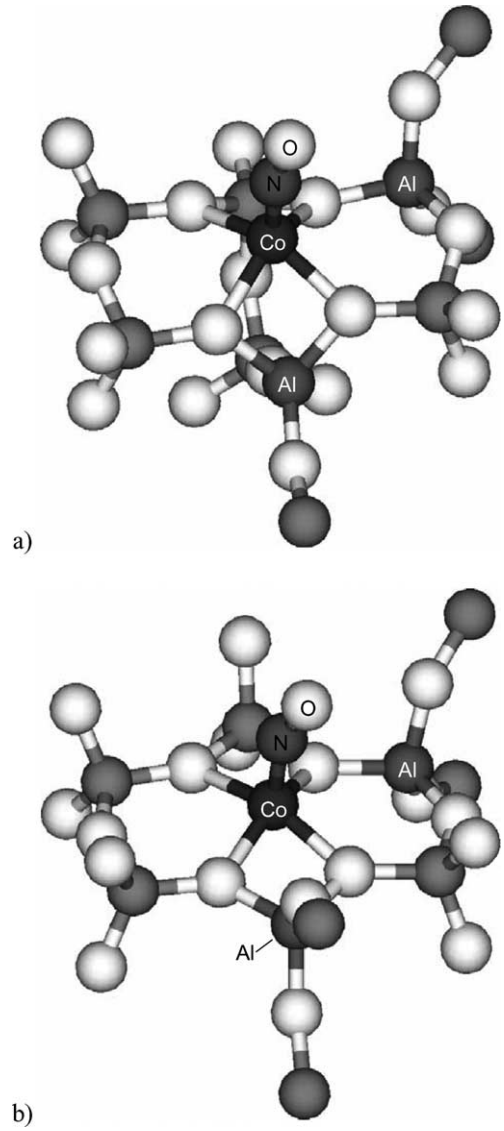

Fig. 2. Structures of the cobalt–mononitrosyl complex in the (a) B-1,3 and (b) G-1,3 clusters (terminating hydrogen atoms not shown). Unless otherwise labeled, the white atoms are oxygen and the gray atoms are silicon.

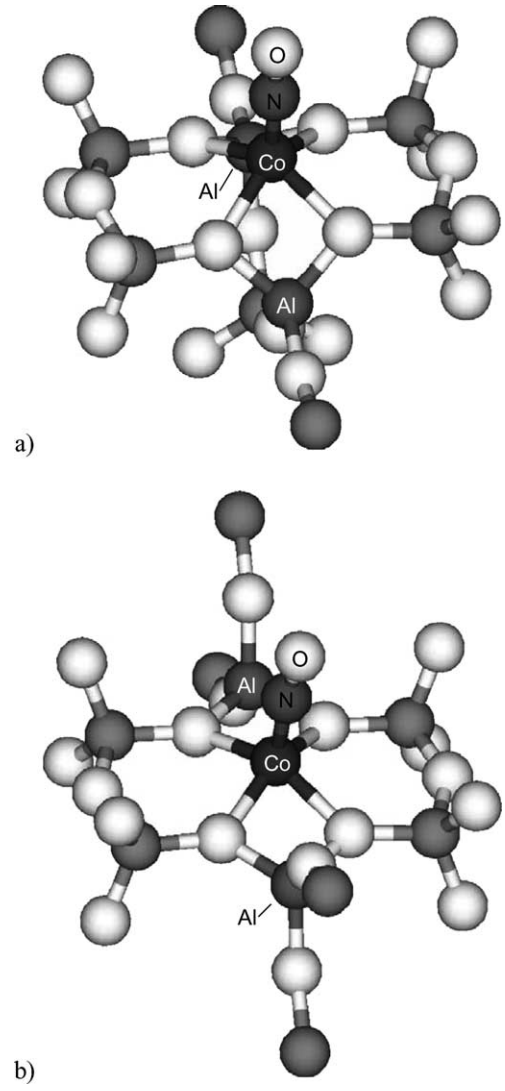

Fig. 3. Structures of the cobalt–mononitrosyl complex in the (a) B-1,4 and (b) G-1,4 clusters (terminating hydrogen atoms not shown).

was used for the light atoms and the remaining heavy atom electrons. Stability calculations confirmed the ground-state configuration of all of the wavefunctions. All calculations were performed with the Gaussian quantum chemical software package [19].

Divalent cobalt cations in zeolites prefer the high-spin (quartet) configuration with three unpaired electrons [5,6,13]. NO also has an unpaired electron localized on nitrogen (doublet). Hence, the mononitrosyl adsorption complex has three possible spin states: singlet, triplet, and quintet. In all cases, the electronic energy of the optimized triplet adsorption complex was lower than the energy of the optimized singlet or quintet complexes. Only the triplet spin configuration is observed experimentally [20], and only the triplet results are discussed below.

3. Results and discussion

3.1. Structure

The lowest energy mononitrosyl adsorption complexes for the clusters are shown in Figs. 2–6. In each case, NO adsorbs through the nitrogen atom. Adsorption through the oxygen atom was always less favorable. Table 1 shows that the cobalt–nitrogen distance is slightly longer for the G environments than the B environments, but not significantly; the cobalt–nitrogen distance is slightly shorter for all of the zeolite environments compared to the cobalt–water environment. NO adsorbs with a linear orientation for some of the environments but is bent for others [21]. The environments with rotationally symmetric aluminum distributions with respect to the cobalt–nitrogen bond, i.e., (1,4) and (2,5), are linear, while environments with nonsymmetric aluminum distributions, i.e., (1,3) and (2,6), are bent. Linear versus

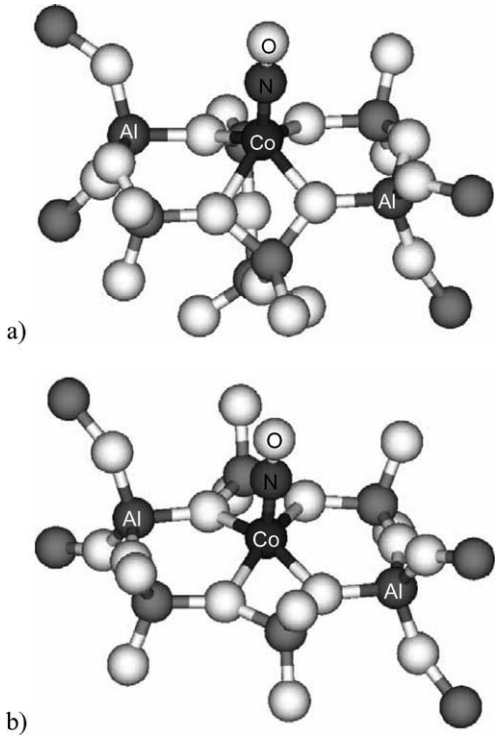

Fig. 4. Structures of the cobalt–mononitrosyl complex in the (a) B-2,5 and (b) G-2,5 clusters (terminating hydrogen atoms not shown).

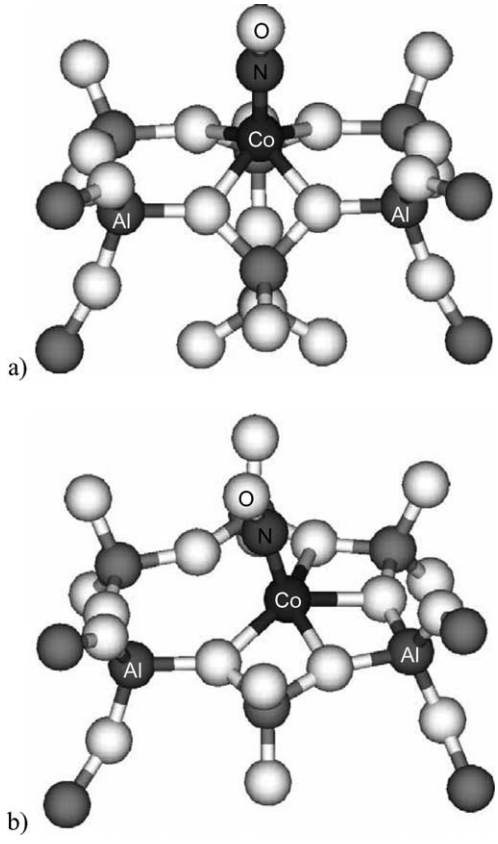

Fig. 5. Structures of the cobalt–mononitrosyl complex in the (a) B-2,6 and (b) G-2,6 clusters (terminating hydrogen atoms not shown).

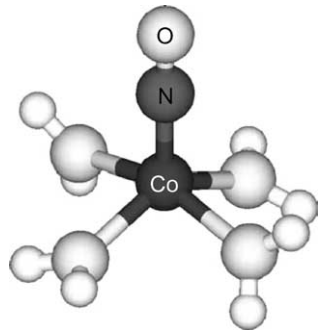

Fig. 6. Structure of the cobalt–mononitrosyl complex formed by divalent cobalt surrounded by four water molecules. Hydrogen atoms are represented by small white spheres.

Table 1
Cobalt–nitrosyl geometries

Environment	Co–N (Å)	Co–N–O (deg)
$[Co(H_2O)_4]^{2+}$	1.75	180
B-1,3	1.71	169
B-1,4	1.70	180
B-2,5	1.70	180
B-2,6	1.70	168
G-1,3	1.73	159
G-1,4	1.72	174
G-2,5	1.73	180
G-2,6	1.72	164

Table 2
NBO partial charges of the cobalt–nitrosyl adsorption complex and the individual cobalt–zeolite and NO components

Environment	Initial				Adsorbed			
	Co	Z	N	O	Co	Z	N	O
$[Co(H_2O)_4]^{2+}$	1.47	0.53[a]	0.18	−0.18	1.26	0.51[a]	0.14	0.09
B-1,3	1.39	−1.39	0.18	−0.18	1.22	−1.27	0.11	−0.06
B-1,4	1.38	−1.38	0.18	−0.18	1.23	−1.28	0.11	−0.06
B-2,5	1.40	−1.40	0.18	−0.18	1.22	−1.29	0.11	−0.04
B-2,6	1.38	−1.38	0.18	−0.18	1.20	−1.27	0.11	−0.04
G-1,3	1.37	−1.37	0.18	−0.18	1.23	−1.30	0.12	−0.05
G-1,4	1.38	−1.38	0.18	−0.18	1.24	−1.32	0.13	−0.05
G-2,5	1.41	−1.41	0.18	−0.18	1.26	−1.38	0.14	−0.03
G-2,6	1.43	−1.38	0.18	−0.18	1.24	−1.31	0.11	−0.05

[a] Total charge on the four water molecules.

bent metal–nitrosyl orientations are sometimes interpreted in terms of the NO charge or number of electrons [22,23]. A positively charged mononitrosyl should adopt a linear orientation, while a negatively charged mononitrosyl will be bent. Table 2 shows that the adsorbed NO natural bond order (NBO) charges vary from 0.05 to 0.11 but are uniformly positive for all of the environments. The NO charge thus does not determine the metal–nitrosyl angle for cobalt-exchanged zeolites. The origin of the Co–N–O bending will be addressed further in the later section on molecular orbital interactions.

Table 3
Overall NO adsorption energies with the individual contributions from zeolite strain and Co–NO bonding (kJ/mol)

Environment	ΔE_{ads}	ΔE_{bond}	ΔE_{strain}	ECN[a]
$[Co(H_2O)_4]^{2+}$	−121	–	–	4.2
B-1,3	−176	−182	+6	4.2
B-1,4	−167	−175	+8	4.2
B-2,5	−182	−189	+7	4.1
B-2,6	−185	−190	+5	4.2
G-1,3	−130	−162	+32	4.6
G-1,4	−127	−162	+35	4.5
G-2,5	−126	−155	+29	4.6
G-2,6	−135	−169	+34	4.4

[a] Electronic coordination number of cobalt w/o adsorbed NO.

3.2. Energetics

The adsorption energy, ΔE_{ads}, is the difference in the SCF electronic energy of the products and reactants:

$$(Z\text{–}Co)_i + NO \xrightarrow{\Delta E_{ads}} Z\text{–}Co\text{–}NO. \quad (1)$$

$(Z–Co)_i$ is the initial bare cobalt environment and Z–Co–NO is the cobalt environment with NO adsorbed. Like the structural parameters, the adsorption energy also depends on the cobalt extraframework site. The adsorption energies in Table 3 broadly divide into two groups according to the extraframework B and G sites. Adsorption is favored by approximately 50 kJ/mol on the B clusters over the G clusters.

Much of the difference in adsorption energy between the B and G sites is attributable to structural differences between cobalt in the two sites. Regardless of the cluster, the four framework oxygen atoms coordinated to cobalt form a plane that is parallel to the *xy*-plane in the coordinate system of the clusters; additionally, the entire six-membered ring of the G site is planar. In the absence of any adsorbed molecules, cobalt in the G site lies in the plane of framework oxygen atoms. Bare cobalt in the B site is located above the plane of the oxygen atoms at the apex of a pyramid formed by cobalt and the four oxygen atoms. Fig. 7 shows the increase in energy due to the change in the vertical position of cobalt from its position in the optimized geometry in the G-1,3 and B-1,4 environments without adsorbed NO. To obtain Fig. 7, the vertical cobalt position was fixed at specified values while the rest of the cluster was allowed to relax except for the usual fixed terminating groups. While the energetic penalty corresponding to a given vertical cobalt displacement is larger for the B-1,4 environment than the G-1,3 environment, the actual vertical displacement of cobalt is much larger in the G environments than the B environments when NO adsorbs. The vertical position of cobalt in the B site changes minimally, less than 0.1 Å, as a result of NO adsorption. However, NO pulls cobalt out of the G site oxygen plane by 0.5 to 0.6 Å, depending on the G cluster. The energetic penalty corresponding to the vertical position of cobalt in the G-1,3 environment after NO adsorption is thus 20 to 30 kJ/mol from Fig. 7.

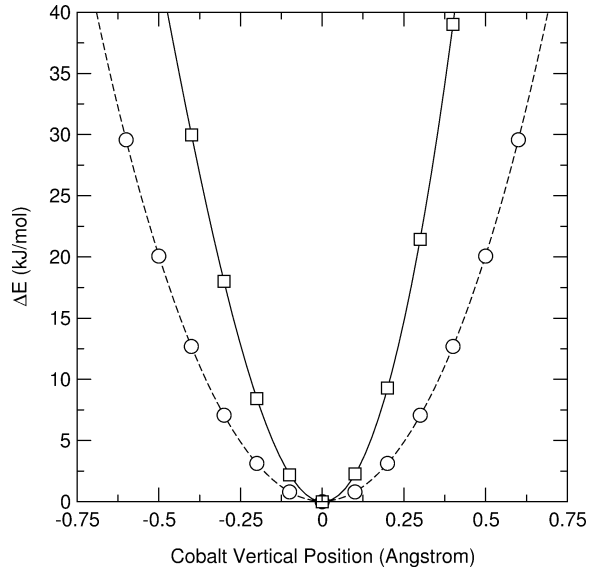

Fig. 7. The increase in energy (kJ/mol) with respect to the fixed vertical position of cobalt in the B-1,4 (□) and G-1,3 (○) environments without adsorbed NO. The zero position corresponds to the minimum energy position of cobalt in each environment. Positive displacement is directed toward the zeolite channel.

The cobalt vertical displacement is the most distinguishable, but not the only, structural change that occurs as a result of NO adsorption. The energy penalty due to zeolite structural changes that occur upon adsorption was quantified by decomposing the adsorption energy, ΔE_{ads}, into two components, the strain energy, ΔE_{strain}, and the Co–NO bond energy, ΔE_{bond}:

$$(Z\text{–}Co)_i + NO \xrightarrow{\Delta E_{strain}} (Z\text{–}Co)_f + NO, \quad (2)$$

$$(Z\text{–}Co)_f + NO \xrightarrow{\Delta E_{bond}} Z\text{–}Co\text{–}NO. \quad (3)$$

$(Z–Co)_i$ is the minimum energy geometry of the bare cobalt environment while $(Z–Co)_f$ has the same geometry as the adsorbed environment (Z–Co–NO) but without the adsorbed NO molecule. Hence, the strain energy measures how significantly the structure of the zeolite changes as a result of NO adsorption. The strain energy and bond energy sum to the overall adsorption energy; the bond energy provides a better indicator of the intrinsic Co–NO bond strength than the adsorption energy since it does not include the effect of strain.

All three energies are reported in Table 3. The adsorption-induced strain is ∼ 25 kJ/mol larger for the G sites than the B sites. The cobalt vertical displacement is a large fraction of the strain energy, but it is not the only contributing factor; however, the other contributions to the strain energy cannot be attributed to any other one specific structural distortion. The strain difference does not completely account for the ∼ 50 kJ/mol difference in the adsorption energies between the two environments. The bond energy differences indicate that adsorption is intrinsically favored on the B environments over the G environments by ∼ 20 kJ/mol. The source of this

difference is most likely differences in the coordinative unsaturation of the cobalt cation depending on the ferrierite environment. Using the molecular orbital overlap populations to define an electronic coordination number [24], cobalt is more coordinatively unsaturated in the B site than the G site (Table 3). The overall difference in the adsorption energies for the B and G sites is the sum of the intrinsic difference and the NO-induced strain on the cobalt–ferrierite.

3.3. Thermodynamics

The default vibrational modes produced by Gaussian were used to calculate the enthalpy, entropy, and free energy of adsorption and are reported in Table 4 under the heading Before level shift. These quantities are computed at a specific temperature via corrections to the electronic energy [25] and are reported here at 298 K. The enthalpies follow the same general pattern as the adsorption energies, with a large difference between the B and the G sites. The adsorption entropies vary by almost 100 J/(mol K) with a standard deviation of nearly 30 J/(mol K). As a result of the variation in the values of ΔS, the trends in the free energy do not mirror the trends in the enthalpy. For instance, the B site enthalpies of adsorption vary by over 20 kJ/mol, yet the largest difference in the free energies is 7 kJ/mol. The wide variation in the values of ΔS is surprising considering that NO always binds to cobalt through nitrogen with an end-on orientation. The reduction in the degrees of freedom for NO and the zeolite should be very similar for all of the clusters.

The clusters are terminated by hydrogen atoms; this is an artificial condition required for cluster calculations. In addition, the terminal groups of the clusters are fixed and not allowed to relax. Both of these termination conditions significantly affect the calculated vibrational modes. Many of the modes are imaginary, owing to the fixed atoms, while many of the nonimaginary modes are spurious due to the coupling between the artificial termination groups and the rest of the cluster. These problematic vibrations can be removed by a force constant level-shifting technique [13]. The Hessian matrix elements corresponding to the fixed atoms are shifted to very large positive values. As a result, the vibrations corresponding to the frozen atoms are shifted to very large frequencies, greater than 10,000 cm^{-1}, that are then discarded. Since three of the thermodynamic correction terms are functions of the vibrational frequencies, the set of level-shifted frequencies should provide improved thermodynamic quantities. The zero point energy (ZPE) and the vibrational corrections to the enthalpy (ΔH_{vib}) and entropy (ΔS_{vib}) are summations over the vibrational frequencies, ν_i [25],

$$\mathrm{ZPE} = \sum_i^M \frac{1}{2} h\nu_i, \tag{4}$$

$$\Delta H_{vib} = \sum_i^M \frac{h\nu_i}{\exp\left(\frac{h\nu_i}{kT}\right) - 1}, \tag{5}$$

$$\Delta S_{vib} = k \sum_i^M \left\{ \frac{h\nu_i/kT}{\exp\left(\frac{h\nu_i}{kT}\right) - 1} - \log\left[1 - \exp\left(-\frac{h\nu_i}{kT}\right)\right]\right\}, \tag{6}$$

where h is Planck's constant, k is Boltzmann's constant, T is the temperature, and M is the number of nonimaginary vibrational modes. Before applying the level-shifting technique, the numerical value of M is between $3n - 6$ and $3N - 6$, where n is the number of unconstrained atoms and N is the total number of atoms. The number of vibrational modes is exactly $3n - 6$ after applying the level-shifting technique.

The enthalpy, entropy, and free energy of adsorption corresponding to the level-shifted frequencies are given in Table 4. The largest difference in the entropies is reduced to 28 J/(mol K). The standard deviation also decreases substantially to slightly less than 9 J/(mol K). In addition, the change in the entropy for the zeolite environments is very similar to the cobalt–water environment, which was not affected by the level shift since no atoms are fixed in that environment. The similarity in the corrected values of ΔS agrees with the similar reductions that are expected in the NO degrees of freedom upon adsorption for all of the clusters. As a result, the trends in the free energies of adsorption generally agree with the enthalpies. The broad energetic distinction between the B and G clusters is still present in the level-shifted enthalpies and free energies. However, within the B clusters, another division may be warranted. The free energy of NO adsorption is about 10 kJ/mol less favorable on the B-1,3 and B-1,4 clusters compared to the B-2,5 and B-2,6 clusters. This further distinction suggests that three classes of cobalt environments exist in terms of enthalpy and free energy. However, this difference is much smaller than the overall difference between the B and the G sites and falls within the accuracy of the calculations.

Table 4
Computed thermodynamics before and after applying the level-shift vibrational correction

Environment	Before level shift			After level shift		
	ΔH_{298} kJ/mol	ΔS_{298} J/(mol K)	ΔG_{298} kJ/mol	ΔH_{298} kJ/mol	ΔS_{298} J/(mol K)	ΔG_{298} kJ/mol
$[Co(H_2O)_4]^{2+}$	−92	−149	−49	−92[a]	−149[a]	−49[a]
B-1,3	−141	−124	−104	−140	−150	−95
B-1,4	−133	−89	−107	−137	−166	−88
B-2,5	−149	−133	−110	−148	−156	−102
B-2,6	−155	−161	−107	−151	−161	−103
G-1,3	−99	−136	−58	−97	−156	−51
G-1,4	−95	−108	−62	−93	−150	−48
G-2,5	−97	−180	−44	−92	−138	−51
G-2,6	−98	−121	−62	−101	−159	−53

The BSSE correction is applied to both sets of values.

[a] Since no atoms are fixed in this environment, the level shift has no effect.

3.4. Temperature-programmed desorption

The impact of the atomic-scale heterogeneities on the macroscopic scale can be evaluated by simulating the temperature-programmed desorption (TPD) profile of each cluster independently. The adsorption and desorption rates were determined using the calculated thermodynamic values, corrected for basis set superposition error [26], and assuming that the initial NO coverage on each cluster was the same. The preexponential factor of the desorption rate constant was assumed to be a constant at 10^{13} s^{-1}, and the adsorption was assumed to be unactivated [27]. The adsorption rate constant was then determined from the thermodynamic consistency relation.

$$k_a = A_a, \tag{7}$$

$$k_d = A_d \exp\left(\frac{\Delta H_{ads}}{RT}\right), \tag{8}$$

$$\frac{k_a}{k_d} = \frac{1}{C^0} \exp\left(\frac{-\Delta G_{ads}}{RT}\right), \tag{9}$$

where k_a and k_d are the adsorption and desorption rate constants, respectively, A_a and A_d are the adsorption and desorption preexponential factors, respectively, and C^0 is the standard-state concentration. The operating parameters, such as the total flow rate and temperature ramp, were taken from Li and Armor [4].

The three broad classes of thermodynamic values in Table 4 are sufficiently distinct to produce three different TPD profiles shown in Fig. 8. The Type I peak is characteristic of NO desorption from all four of the G clusters. Unlike the G clusters, the B clusters split into two desorption peaks. The B-1,3 and B-1,4 clusters correspond to the Type II peak, and the B-2,5 and B-2,6 clusters correspond to the Type III peak. The relatively small enthalpic difference between the B-1,3/B-1,4 clusters versus the B-2,5/B-2,6 clusters is sufficient to separate the NO desorption peaks. This difference is within the accuracy of the calculations, but if real, could be observed at the macroscopic level. The large difference between the B and the G sites, however, is quite clearly seen.

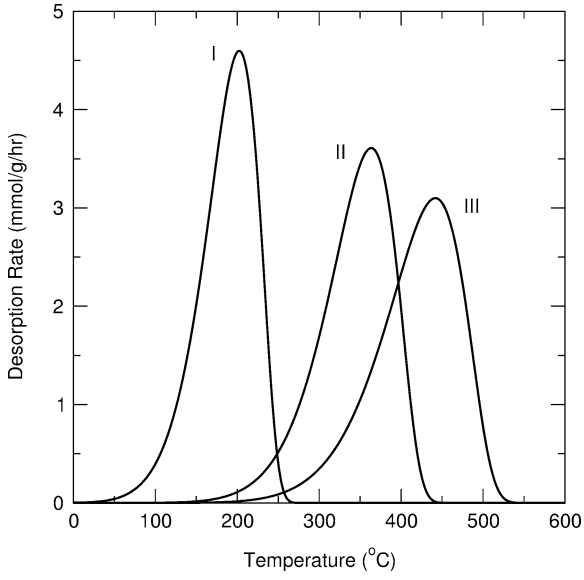

Fig. 8. Simulated NO temperature-programmed desorption profiles corresponding to (I) all of the G clusters (represented by G-1,3 in the figure), (II) the B-1,3 and B-1,4 clusters (represented by B-1,4), and (III) the B-2,5 and B-2,6 clusters (represented by B-2,5). The following simulation parameters were taken from Li and Armor [4]: total molar flow rate = 7.44×10^{-5} mol He/s, total pressure = 1.01 bar, cobalt cations = 4.82×10^{19} sites, reactor volume = 0.2 cm^3, and temperature ramp = 0.133 °C/s.

3.5. Electron transfer and orbital interactions

The partial charges listed in Table 2 show that upon adsorption of NO the net charge decreases on cobalt with corresponding charge increases on NO and the zeolite. Adsorbed NO has a small dipole with a net positive charge. As Table 2 suggests, the electron transfer is very similar for all of the clusters despite all of their other differences. Table 5 shows that the spin densities, the difference in the number of spin up and spin down electrons, are also very similar among all of the clusters.

The change in electron density upon adsorption shown in Fig. 9 reveals that the cobalt–nitrosyl bond is mostly a π-type interaction between the cobalt d and nitrogen p orbitals. A natural orbital bonding analysis on the B-1,4 cluster confirms this type of interaction. The significant changes in the cobalt orbital occupations occur in the three d orbitals with z-polarization: d_{xz}, d_{yz}, and d_{zz}. The cobalt–nitrogen bond is aligned with the z-axis in the coordinate system of all the clusters. The total change in the electron number in these orbitals almost completely accounts for the net change in the cobalt partial charge and spin density upon adsorption (Tables 2 and 5). Cobalt in the absence of the nitrosyl ligand has a $4s^{0.22}3d^{7.38}$ electronic structure which changes to $4s^{0.24}3d^{7.51}$ after adsorption of NO.

Fig. 10 shows the molecular orbital overlap population (MOOP) [28] as a function of orbital energy relative to the highest occupied molecular orbital (HOMO). MOOP diagrams provide valuable insight into the nature of chemical bonds; positive peaks indicate bonding orbital interac-

Table 5
NBO spin densities of the cobalt–nitrosyl adsorption complex and the individual cobalt–zeolite and NO components

Environment	Initial				Adsorbed			
	Co	Z	N	O	Co	Z	N	O
$[Co(H_2O)_4]^{2+}$	2.67	0.33[a]	0.70	0.30	2.15	0.30[a]	−0.17	−0.28
B-1,3	2.57	0.43	0.70	0.30	2.01	0.45	−0.20	−0.26
B-1,4	2.57	0.43	0.70	0.30	2.04	0.46	−0.22	−0.28
B-2,5	2.57	0.43	0.70	0.30	2.02	0.46	−0.21	−0.27
B-2,6	2.55	0.45	0.70	0.30	1.97	0.46	−0.18	−0.25
G-1,3	2.58	0.42	0.70	0.30	2.04	0.43	−0.21	−0.27
G-1,4	2.58	0.42	0.70	0.30	2.07	0.44	−0.23	−0.29
G-2,5	2.62	0.38	0.70	0.30	2.12	0.38	−0.23	−0.28
G-2,6	2.60	0.40	0.70	0.30	2.02	0.43	−0.20	−0.26

[a] Total spin density on the four water molecules.

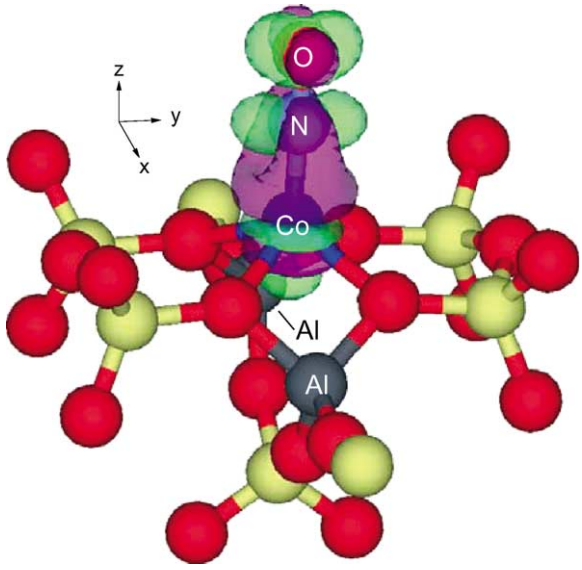

Fig. 9. Electron density difference due to NO adsorption on cobalt in the B-1,4 environment. Purple regions correspond to increases in electron density and green regions correspond to decreases in electron density. One of the lobes of the d_{zz}-like density decrease is hidden behind the d_{xz} and d_{yz}-like density increase. The surface corresponds to a change in electron density of 0.002 electrons. Oxygen atoms are red, silicon atoms are gold, and aluminum atoms are gray.

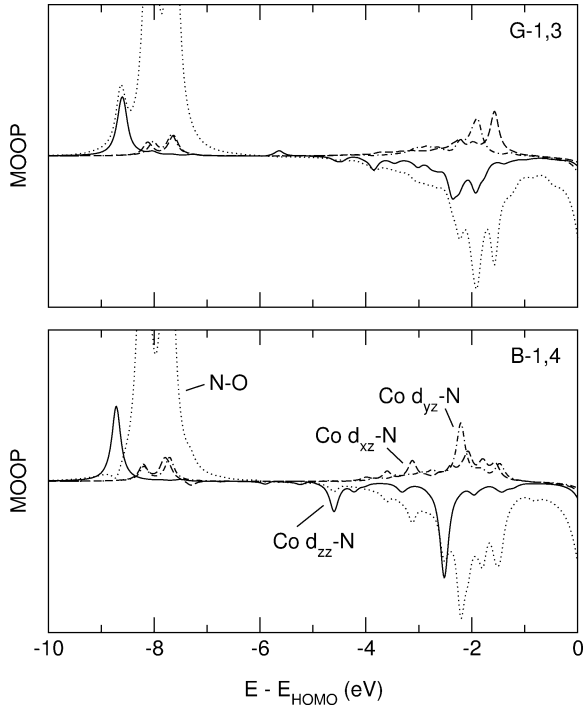

Fig. 10. Molecular orbital overlap population (MOOP) diagrams for the G-1,3 (top) and B-1,4 (bottom) environments. The cobalt–nitrogen MOOP interactions are shown for the cobalt d_{zz} (solid), d_{xz} (dashed), and d_{yz} (dash-dot) orbitals. The nitrogen–oxygen MOOP (dotted) is also shown. The cobalt d_{xz} and d_{yz} bonding orbitals are almost entirely spin up, while the antibonding d_{zz}-nitrogen interaction is primarily through spin-down orbitals. The antibonding nitrogen–oxygen interactions are a mix of spin-up and spin-down orbitals.

tions while negative peaks indicate antibonding orbital interactions. In the cobalt d-band region (between −6 and 0 eV), the cobalt d_{xz} and d_{yz} orbitals contribute to the cobalt–nitrogen bond, while the cobalt d_{zz} orbital has an antibonding interaction with nitrogen. The cobalt–nitrogen orbital interactions are remarkably similar for the B-1,4 and G-1,3 environments as shown in Fig. 10. All of the environments share similar features in electronic structure and orbital population changes. These similarities demonstrate that the character of the cobalt–nitrogen bond is also similar regardless of the environment. The total integrated MOOP between cobalt and the four framework oxygen atoms was used to calculate the electronic coordination number [24]. Cobalt in the B site is more coordinatively unsaturated than cobalt in the G (Table 3). Hence, the ∼ 20 kJ/mol difference in the bond energy [Eq. (3)] between the B and the G sites is most likely due to the relative coordinative unsaturation of the B site compared to the G site.

The linear versus bent adsorbed NO orientations may also be understood by examining features of the electronic structure. The relative position of the antibonding Co–NO orbitals determines whether NO is bent or linear [22]; these orbitals are shown in Fig. 11 for the B-1,4 and G-1,3 environments. The antibonding d_{zz} orbital shifts toward the HOMO orbital upon adsorption in the bent nitrosyl environment (G-1,3), but shifts to lower energy in the linear nitrosyl environment (B-1,4) (Fig. 11b). Additionally, the antibonding N–O orbitals are closer to the HOMO orbital energy

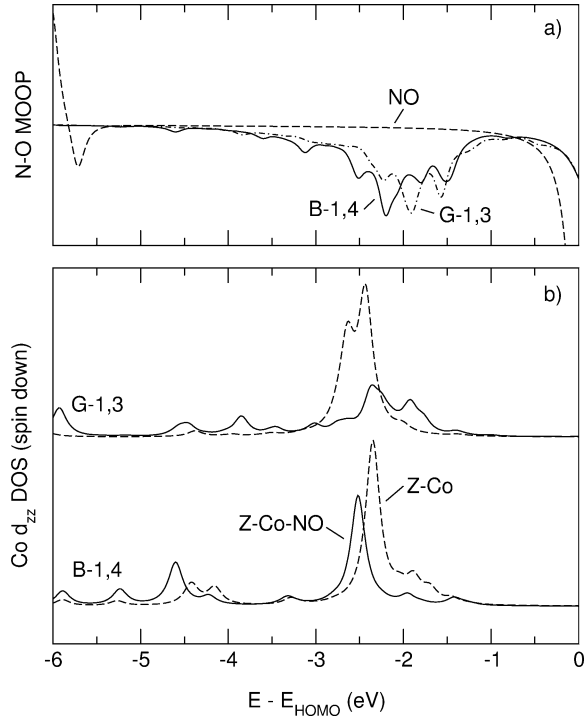

Fig. 11. (a) Nitrogen–oxygen molecular orbital overlap population (MOOP) for the B-1,4 and G-1,3 environments and gas-phase NO and (b) spin-down d_{zz} cobalt orbital density of states (DOS) before (dashed) and after (solid) NO adsorption for the B-1,4 and G-1,3 environments.

for the G-1,3 environment compared to the B-1,4 environment (Fig. 11a). The environments with nonsymmetric aluminum distributions, i.e., (1,3) and (2,6), shift these orbitals to higher energy and form bent nitrosyls, while the symmetric aluminum environments, i.e., (1,4) and (2,5), shift these orbitals to lower energy and form linear nitrosyls.

4. Conclusions

Quantum chemical calculations have shown that NO adsorbs favorably to cobalt in two ferrierite extraframework sites. The orbital interactions between cobalt, the zeolite, and NO are similar for all of the sites investigated. Despite these similarities, the mononitrosyl geometries and enthalpies of adsorption differ among the clusters depending on the structural features of the zeolite near cobalt. Sites with symmetric distributions of aluminum atoms favor linear nitrosyl orientations. A lack of aluminum symmetry results in bent mononitrosyls. The linear versus bent configurations are due to differences in the antibonding Co–N–O orbitals. NO adsorption to cobalt in the B site is approximately 50 kJ/mol more favorable than to cobalt in the G site. This difference is partly attributable to the greater strain that adsorbed NO places on the G site than the B site. The remaining $\sim$ 20 kJ/mol difference is intrinsic to the sites and is most likely due to the greater degree of coordinative unsaturation of cobalt in the B site compared to the G site.

The level-shifted vibrational modes were shown to yield improved thermodynamic values compared to the sets of modes that include contributions from the artificial cluster termination. The calculated thermodynamics divide the clusters into three classes of cobalt environments, each of which is observable in the simulated temperature-programmed desorption profile. Hence, local zeolite framework heterogeneity near cobalt has a strong influence on the macroscopic properties of NO adsorption on cobalt–ferrierite. This suggests that the catalytic activity of cobalt-exchanged zeolites for the selective catalytic reduction of NO_x may also depend on the same factors: adsorption-induced strain and intrinsic metal coordination differences.

Acknowledgments

The authors thank Wolfgang Sachtler for many insightful discussions on SCR catalysis and two anonymous reviewers for their helpful comments. This work was supported by the EMSI program of the National Science Foundation and the Department of Energy (CHE-9810378) at the Northwestern University Institute for Environmental Catalysis. Additional support was provided by the National Computational Science Alliance (CTS010016N) utilizing the NCSA Origin 2000.

References

[1] Y. Traa, B. Burger, J. Weitkamp, Micropor. Mesopor. Mater. 30 (1999) 3.
[2] Y. Li, J.N. Armor, Appl. Catal. B 1 (1992) L31.
[3] J.N. Armor, Catal. Today 26 (1995) 147.
[4] Y. Li, J.N. Armor, J. Catal. 150 (1994) 376.
[5] Y. Li, T.L. Slager, J.N. Armor, J. Catal. 150 (1994) 388.
[6] E.-M. El-Malki, D. Werst, P.E. Doan, W.M.H. Sachtler, J. Phys. Chem. B 104 (2000) 5924.
[7] X. Wang, H.-Y. Chen, W.M.H. Sachtler, Appl. Catal. B 26 (2000) L227.
[8] X. Wang, H. Chen, W.M.H. Sachtler, Appl. Catal. B 29 (2001) 47.
[9] D. Kaucký, J. Dědeček, B. Wichterlová, Micropor. Mesopor. Mater. 31 (1999) 75.
[10] D. Kaucký, A. Vondrová, J. Dědeček, B. Wichterlová, J. Catal. 194 (2000) 318.
[11] J. Dědeček, D. Kaucký, B. Wichertlová, Top. Catal. 18 (2002) 283.
[12] W.J. Mortier, Compilation of Extra Framework Sites in Zeolites, Butterworth, London, 1982.
[13] S.A. McMillan, L.J. Broadbelt, R.Q. Snurr, J. Phys. Chem. B 106 (2002) 10864.
[14] K. Pierloot, A. Delabie, M.H. Groothaert, R.A. Schoonheydt, Phys. Chem. Chem. Phys. 3 (2001) 2174.
[15] A. Delabie, K. Pierloot, M.H. Groothaert, B.M. Weckhuysen, R.A. Schoonheydt, Phys. Chem. Chem. Phys. 4 (2002) 134.
[16] Z. Sobalík, J. Dědeček, B. Wichterlová, L. Drozdová, R. Prins, J. Catal. 194 (2000) 330.
[17] A.D. Becke, Phys. Rev. A 38 (1988) 3098.
[18] J.P. Perdew, Phys. Rev. B 33 (1986) 8822.
[19] M.J. Frisch, G.W. Trucks, H.B. Schlegel, G.E. Scuseria, M.A. Robb, J.R. Cheeseman, V.G. Zakrzewski, J.A. Montgomery, R.E. Stratmann, J.C. Burant, S. Dapprich, J.M. Millam, A.D. Daniels, K.N. Kudin, M.C. Strain, O. Farkas, J. Tomasi, V. Barone, M. Cossi, R. Cammi, B. Mennucci, C. Pomelli, C. Adamo, S. Clifford, J. Ochterski, G.A. Petersson, P.Y. Ayala, Q. Cui, K. Morokuma, N. Rega, P. Salvador, J.J. Dannenberg, D.K. Malick, A.D. Rabuck, K. Raghavachari, J.B. Foresman, J. Cioslowski, J.V. Ortiz, A.G. Baboul, B.B. Stefanov, G. Liu, A. Liashenko, P. Piskorz, I. Komaromi, R. Gomperts, R.L. Martin, D.J. Fox, T. Keith, M.A. Al-Laham, C.Y. Peng, A. Nanayakkara, M. Challacombe, P.M.W. Gill, B. Johnson, W. Chen, M.W. Wong, J.L. Andres, C. Gonzalez, M. Head-Gordon, E.S. Replogle, J.A. Pople, Gaussian 98, Revision A.11.3, Gaussian, Inc., Pittsburgh, PA, 2002.
[20] S.-K. Park, V. Kurshev, C.W. Lee, L. Kevan, Appl. Magn. Reson. 19 (2000) 21.
[21] The Co–N–O angles of the "bent" cobalt–nitrosyls observed here are between 159 and 169°. These bending angles are relatively small compared to other bent metal–nitrosyls which typically have angles of $\sim$ 130°. See Ref. [22] and references therein.
[22] J.H. Enemark, R.D. Feltham, Coord. Chem. Rev. 13 (1974) 339.
[23] W.F. Schneider, K.C. Hass, R. Ramprasad, J.B. Adams, J. Phys. Chem. B 100 (1996) 6032.
[24] W.T. Lee, L. Ford, P. Blowers, H.L. Nigg, R.I. Masel, Surf. Sci. 416 (1998) 141.
[25] D.A. McQuarrie, Statistical Mechanics, Harper & Row, New York, 1976.
[26] F.B. van Duijneveldt, J.G.C.M. van Duijneveldt-van de Rijdt, J.H. van Lenthe, Chem. Rev. 94 (1994) 1873.
[27] S.B. Sharma, B.L. Meyers, D.T. Chen, J. Miller, J.A. Dumesic, Appl. Catal. A 102 (1993) 253.
[28] R. Hoffmann, Solids and Surfaces: A Chemist's View of Bonding in Extended Structures, VCH, New York, 1988.